The VASP tetramerization domain is a right-handed coiled coil based on a 15-residue repeat

Karin Kühnel*†, Thomas Jarchau‡, Eva Wolf*, Ilme Schlichting†, Ulrich Walter‡§, Alfred Wittinghofer*§, and Sergei V. Strelkov¶

*Max-Planck-Institut für Molekulare Physiologie, Abteilung Strukturelle Biologie, Otto-Hahn-Strasse 11, 44227 Dortmund, Germany; ‡Institut für Klinische Biochemie und Pathobiochemie, Josef Schneider Strasse 2, 97080 Würzburg, Germany; †Max-Planck-Institut für Medizinische Forschung, Abteilung Biomolekulare Mechanismen, Jahnstrasse 29, 69120 Heidelberg, Germany; and ¶Maurice E. Müller Institute for Structural Biology, Biozentrum, University of Basel, Klingelbergstrasse 70, CH-4056 Basel, Switzerland

Edited by Carolyn Cohen, Brandeis University, Waltham, MA, and approved October 15, 2004 (received for review May 11, 2004)

The vasodilator-stimulated phosphoprotein (VASP) is a key regulator of actin dynamics. We have determined the 1.3-Å resolution crystal structure of the 45-residue-long tetramerization domain (TD) from human VASP. This domain forms a right-handed α-helical coiled-coil structure with a similar degree of supercoiling as found in the widespread left-handed coiled coils with heptad repeats. The basis for the right-handed geometry of VASP TD is a 15-residue repeat in its amino acid sequence, which reveals a characteristic pattern of hydrophobic residues. Hydrophobic interactions and a network of salt bridges render VASP TD highly thermostable with a melting point of 120°C.

In an estimated 10% of all proteins (1), α-helical coiled coils are present, and they constitute a principal protein-folding motif. Between two and five α-helices are wound around each other, usually forming a left-handed superhelix (2, 3). The sequences of the left-handed coiled coils are characterized by heptad repeats, $(abcdefg)_n$, where positions *a* and *d* are occupied mostly by apolar residues. The left-handed supercoiling is induced by a small but significant difference between 3.5 residues per turn in a heptad repeat and 3.64 residues per turn in an undistorted α-helix (2), by which the residues in the *a* and *d* positions form a hydrophobic core. Typically, coiled coils are very specific oligomers with high thermodynamic stability, which enables them to function as oligomerization domains in many proteins (4).

In addition to the most common coiled coils with heptad repeats, structures with longer repeats are possible. It is worth noting that in 1951 Pauling *et al.* (5) mentioned the feasibility of other periodicities, including 11-residue repeats (three α-helical turns, 11/3) and 15-residue repeats (15/4). Although researchers have focused almost exclusively on coiled coils with heptad repeats (6), 11-residue repeats were found recently in the tetrabrachion protein from *Staphylothermus marinus* (7). Its crystallographic structure has indeed revealed a parallel four-stranded coiled coil with a slight right-handed supercoiling (8). Moreover, it was suggested that 15-residue repeats would induce a yet more pronounced right-handed supercoiling (6).

Here, we report the crystal structure of the tetramerization domain (TD) from human vasodilator-stimulated phosphoprotein (VASP). This domain includes two consecutive 15-residue (quindecad) repeats, which result in a parallel right-handed coiled-coil structure with a similar degree of supercoiling as observed in the left-handed coiled coils with heptad repeats. Furthermore, we show that VASP TD is stabilized by a hydrophobic interface as well as a network of salt bridges, which yields a highly thermostable structure. Last, we discuss how the TD may function as a regulator of actin assembly.

Materials and Methods

Crystallization and Structure Determination. The TD (residues 336–380) of human VASP was expressed and purified as described (9). Crystals were grown at 20°C by using the hanging-drop method. We mixed 5 μl of the 10 mg/ml VASP TD solution with 5 μl of the reservoir solution containing 35% (wt/vol) polyethylene glycol 400, 0.2 M sodium citrate, and 0.1 M Tris (pH 8.5). Pyramidal crystals grew to a size of 200 × 200 × 500 μm within 2 weeks. Before diffraction data collection, the crystals were flash-cooled in liquid nitrogen without addition of further cryoprotectant.

The crystallographic phasing was done by using the single-wavelength anomalous-dispersion technique. A Leu352Met point mutant of VASP TD was prepared because no methionines are present in the wild type. The leucine-to-methionine mutation was done with the QuikChange site-directed mutagenesis procedure (Strategene) and verified by DNA sequencing. The mutant protein was expressed in minimal medium containing selenomethionine as described (10) and purified in the same way as the wild-type protein, with 5 mM dithioerythritol added to all buffers to prevent the oxidation of selenium. Crystals were grown by mixing 5 μl of 15 mg/ml protein solution with 5 μl of 25% (vol/vol) polyethylene glycol MME550/0.2 M sodium citrate/0.1 M Tris (pH 8.5). The crystals were transferred into 35% (vol/vol) polyethylene glycol MME550/0.2 M sodium citrate/0.1 M Tris (pH 8.5) and flash-cooled in liquid nitrogen.

Diffraction data of both crystals were collected at 100 K at the European Synchrotron Radiation Facility (Grenoble, France) by using beamline ID14–2 at a wavelength of 0.933 Å. The data were processed with DENZO and SCALEPACK (11) (Table 1). The crystals belong to space group I4 with unit cell dimensions of $a = b = 29.7$ Å and $c = 100.2$ Å for the wild type and $a = b = 29.7$ Å and $c = 100.4$ Å for the selenomethionine mutant. There is one protein chain per crystallographic asymmetric unit.

The structure of the selenomethionine mutant was solved to a 1.7-Å resolution by single-wavelength anomalous-dispersion phasing from a single Se site by using CNS (12). An interpretable electron density was obtained after solvent flattening. A poly-alanine model was built subsequently with RESOLVE (13, 14). The program O (15) was used for inspection of the electron-density maps and manual rebuilding of the model. Refinement was carried out with CNS and at later stages with REFMAC5 (16). The mutant structure was refined to an *R* factor of 19.2% and an R_{free} value of 21.1% (Table 1). The phases of the mutant protein were then added to the corresponding reflections of the wild type. By using this phase information, an atomic model of the wild type was built. Refinement was initially done with CNS and later with REFMAC5, including anisotropic B-factor refinement. The quality indicators of the final model are presented in Table 1. Side chains

This paper was submitted directly (Track II) to the PNAS office.

Abbreviations: TD, tetramerization domain; VASP, vasodilator-stimulated phosphoprotein; DSC, differential scanning calorimetry; EVH1/2, Ena-VASP homology 1/2.

Data deposition: The atomic coordinates have been deposited in the Protein Data Bank, www.pdb.org (PDB ID codes 1USE and 1USD for wild type and Leu253Met mutant, respectively).

§To whom correspondence may be addressed. E-mail: u.walter@medizin.uni-wuerzburg.de or alfred.wittinghofer@ mpi-dortmund.mpg.de.

Table 1. Crystallographic data collection and refinement statistics

	Leu352SeMet mutant	Wild type
Data collection		
Resolution limits, Å	25–1.7 (1.76–1.70*)	25–1.3 (1.35–1.30)
Total observations	54,657	95,581
Unique observations	4,555	9,974
Completeness	99.8 (99.8)	98.6 (99.3)
I/σ (I)	37.6 (6.3)	26.7 (4.4)
R_{merge},† %	3.5 (30.9)	2.8 (27.9)
Mean FOM of phases (before/after density modification)	0.31/0.85	
Refinement		
R factor, %	19.2	17.6
R_{free},‡ %	21.1	19.3
Overall B factor, Å^2	22.6	20.2
rms deviation in bond lengths, Å	0.026	0.016
rms deviation in bond angles, °	2.001	1.321
Residues included in the model	338–378	338–377
No. of water molecules	46	57

*Data in parentheses correspond to the highest-resolution bin.

†$R_{\text{merge}} = \sum_{hkl}\sum_{i}|I_i(hkl) - \overline{I(hkl)}|/\sum_{hkl}\sum_{i}I_i(hkl)$.

‡With 5% of reflections in the test set.

of Lys-357 and Lys-361 are flexible and not included in the model. Coordinates were deposited at the Protein Data Bank (PDB ID codes 1USE and 1USD for wild-type VASP TD and Leu352Met mutant, respectively). The figures were prepared by using MOLSCRIPT (17) and BOBSCRIPT (18).

Differential Scanning Calorimetry (DSC) Experiments. DSC experiments were carried out with the VP-DSC microcalorimeter (Microcal, Northampton, MA) equipped with a 0.5-ml cell. The heating rate was 1 K/min. Because the microcalorimeter operates up to a maximal temperature of 130°C, addition of 1 M guanidine hydrochloride was used to reduce the transition midpoint temperature by ≈20°C and allow recording of complete transition spectra between 20°C and 130°C (Fig. 4, which is published as supporting information on the PNAS web site). Protein concentrations varied between 0.15 mg/ml (28 μM) and 1 mg/ml (185 μM).

Results and Discussion

Unique Right-Handed Geometry of VASP TD. Previous NMR studies have suggested that the human VASP TD (residues 336–380) forms a stable α-helical tetramer either in a parallel or head-to-tail arrangement (9). The 1.3-Å crystal structure of the domain presented here is a proof of the parallel orientation. The atomic model was refined to a crystallographic R factor of 17.6% and a free R factor of 19.3% (Table 1). The parallel tetramer resulting from a crystallographic 4-fold axis has a cylindrical shape with a length of 60 Å and a diameter of 25–30 Å, with intimate contacts between the chains (Fig. 1*A*), and 45% of the solvent accessible area of each α-helix is buried within the tetramer interface.

The right-handed coiled-coil geometry of VASP TD is strikingly uniform, revealing a constant supercoiling with a pitch of 185 Å along its length (Fig. 1*A*), as calculated with the program TWISTER (19). The degree of supercoiling is similar to that of the left-handed coiled coils with heptad repeats, such as the four-stranded GCN4-pLI leucine zipper with a pitch of 204 Å (20). In contrast, the two previously determined four-stranded coiled-coil structures with 11-residue repeats, the designed RH4 protein (21), and the tetrabrachion fragment from *S. marinus* (8) (residues 19–52), reveal only a slight supercoiling with pitch values of 840 and 1,280 Å, respectively, which corresponds to a nearly parallel α-helical bundle (see also Fig. 2*D*). Interestingly, the short N-terminal part (residues 4–18) of the tetrabrachion structure reveals a more pronounced right-handed supercoiling with a pitch of 322 Å. This part contains a single four-residue insert into the otherwise regular 11-residue repeat pattern, which can be considered equivalent to the formation of a single 15-residue repeat (6) (Fig. 2*C*) comparable with the repeats in VASP TD described below. The superhelical radius of VASP TD is 7.7 Å, similar to the values between 7.4 and 7.6 Å in the above-mentioned four-stranded coiled coils with heptad or 11-residue repeats.

The 15-Residue Repeat. In the VASP TD sequence, two consecutive repeats of 15 residues are observed (residues 344–358 and 359–373, respectively). Of the 15 positions, seven (47%) contain identical amino acids in the two repeats (positions *a*, *b*, *d*, *e*, *g*, *j*, and *o*) and an additional four (positions *c*, *h*, *i*, and *l)* show replacements preserving the nature of the amino acid (i.e., replacements Arg→Lys preserving the charge and replacements Leu→Ile (two times) and Val→Phe preserving the hydrophobicity (Fig. 2*A*). As a reflection of the high sequence similarity, superimposition of the two 15-residue repeats yields an rms deviation of 0.33 Å in the Cα positions. In addition, residues Leu-374 to Lys-376 downstream of the second repeat appear to be an extension of the repeat pattern because of the conservation of the Leu and Lys residues (Fig. 2*A*).

The 15-residue repeat exhibits a pronounced pattern of hydrophobic residues located in positions *a*, *d*, *h*, and *l*. Together with the aliphatic parts of the lysine side chains found in positions *e*, these residues form the hydrophobic core of VASP TD (Fig. 1 *A* and *B*). The principles of the superhelical-structure formation in proteins with heptad, 11-residue, and 15-residue repeats is shown by the α-helical net diagrams (Fig. 2*D*). A full turn of a regular α-helix contains 3.64 residues (2). If a heptad repeat is present, the total α-helical phase increment (19) per heptad is 360°/3.64 × 7 = 692.3°, which deviates from two full turns (720°) by −27.8° (i.e., −4.0° per residue). Correspondingly, hydrophobic residues in *a* and *d* positions of a heptad repeat form a zigzag-shaped patch on the side of the helix, which makes an angle to its axis (Fig. 2*D*). When these hydrophobic patches come together, a left-handed superhelix is formed. The total α-helical phase increment of 11 residues is 360°/3.64 × 11 =

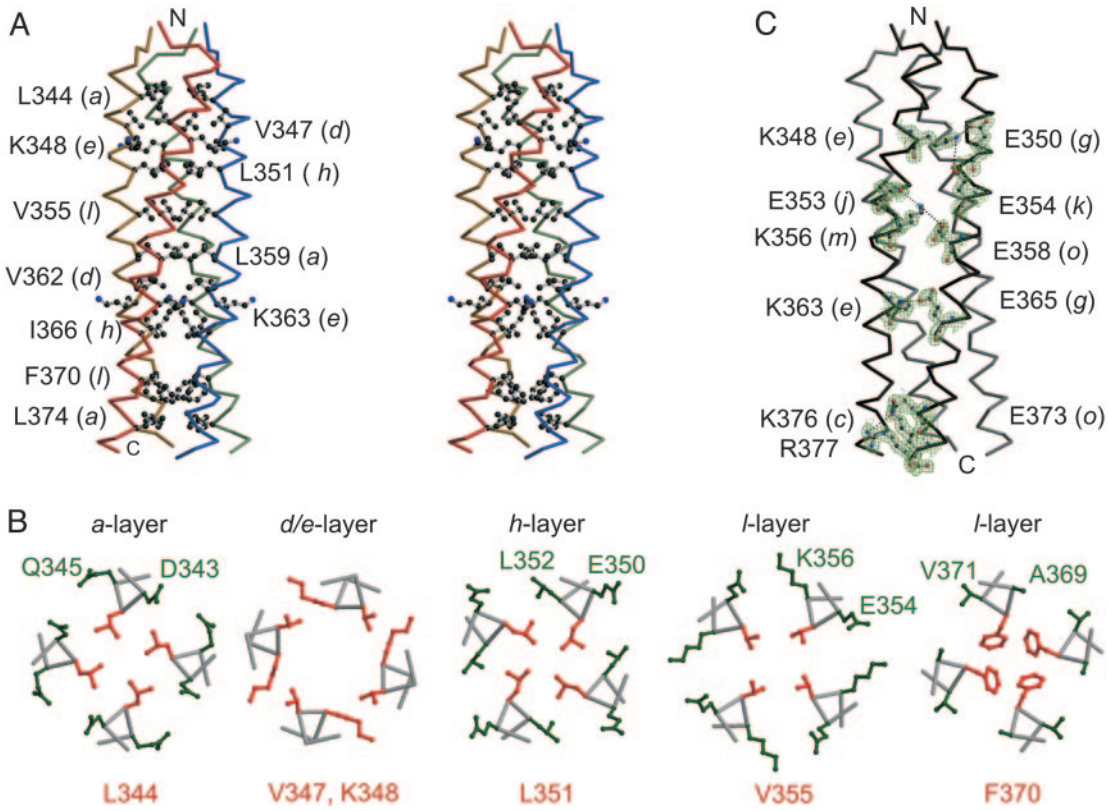

Fig. 1. The VASP TD structure. (*A*) Stereoview of VASP TD. Side chains forming the hydrophobic core are labeled, and the 15-residue repeat positions are marked in parentheses. (*B*) The hydrophobic core packing of VASP TD shown along the tetramer axis from the N-terminal side. Central core layers *a*, *h*, and *l* and the neighbor packing *d*/*e* layer are shown. (*C*) View of VASP TD showing residues that form intrahelical and interhelical salt bridges, together with the corresponding $2F_o - F_c$ electron-density map (contour level, 1.0 σ).

1,087.9°, which exceeds three full turns by 7.9° or only +0.7° per residue, yielding only a slight right-handed supercoiling, as shown in the RH4 and tetrabrachion structures (8, 21). Finally, the 15-residue repeat "overshoots" four full turns by 360°/3.64 × 15–1,440° = 43.5° or +2.9° per residue. Hence, a pronounced right-handed superhelix with a pitch value comparable with those in the left-handed coiled coils should be expected, which is indeed observed in the VASP TD structure (Fig. 2*D*).

At the amino acid sequence level, a 15-residue repeat is equivalent to one heptad repeat and two four-residue insertions (6). Such insertions, called "stutters," are found in many coiled coils with otherwise regular heptad periodicity, and they cause an unwinding of the left-handed coiled coil or even a local switch to a right-handed geometry (19, 22, 23). Thus, VASP TD may be regarded as containing regularly repeated stutters, which are responsible for the pronounced, continuous right-handed supercoiling. In addition, we have now analyzed the two 15-residue repeats of VASP at the structural level by using the program TWISTER, which formally assigns a heptad position to each residue based on structural criteria (19). As shown by this assignment (Fig. 2*A*, bottom row), the two stutter repeats flank the heptad at either side. In other words, the hydrophobic pattern of the VASP repeat can be written as 4-3-4-4 (when using the notation, e.g., in ref. 22).

Hydrophobic Core Packing. The VASP TD structure is stabilized by hydrophobic contacts of two types, which we denote here as the "axial-core" and the "next-neighbor" contacts, respectively (Fig. 1 *A* and *B* and Table 2). The involvement of a side chain in either type of hydrophobic contact correlates with the angle α_{Crick} formed by the C_a-atom position, the corresponding α-helical axis point, and the coiled-coil axis point (3, 19).

Residues belonging to layers *a*, *h*, and *l* have relatively small absolute values of α_{Crick} (Table 2), and they point approximately toward the 4-fold axis of the structure, forming the axial hydrophobic core. Thus, the residues of the *a* layer pack against each other in a "knobs-into-holes" fashion, similar to *a* layers of coiled coils with heptad repeats, which typically have α_{Crick} values close to 20° (19). For example, the side chain of Leu-344 ("knob") fits into the "hole" provided by Leu-344 and the preceding residue Asp-343 of an adjacent helix (Fig. 1*B*). Moreover, the *h* layers of VASP TD also reveal a knobs-into-holes packing (Fig. 1*B*), closely resembling the *d* layers of coiled coils with heptads (typical α_{Crick} value of −30°).

In contrast, the residues in *l* positions feature absolute α_{Crick} values ≤15°. Correspondingly, the side chains from the opposing α-helices point directly to each other, resulting in a "knobs-to-knobs" packing (Fig. 1*B*). Such situation never occurs in coiled coils with regular heptad repeats, but it takes place if heptad stutters are present, resulting in the so-called *x* layers (22, 24). The knobs-to-knobs packing appears to be less favorable energetically than the knobs-into-holes packing. However, this destabilization is likely to be pronounced only in two-stranded and possibly three-stranded coiled coils. In contrast, in four-stranded coiled coils, which have a larger radius, the *l* side chains pack into a fairly compact hydrophobic core (see Fig. 1*B*), with each participating side chain fitting into the relatively small wedge of 90°.

Furthermore, the Val and Lys residues in positions *d* and *e* of VASP TD form a ring of pairwise next-neighbor-type interactions between the adjacent α-helices (Fig. 1 *A* and *B*). These

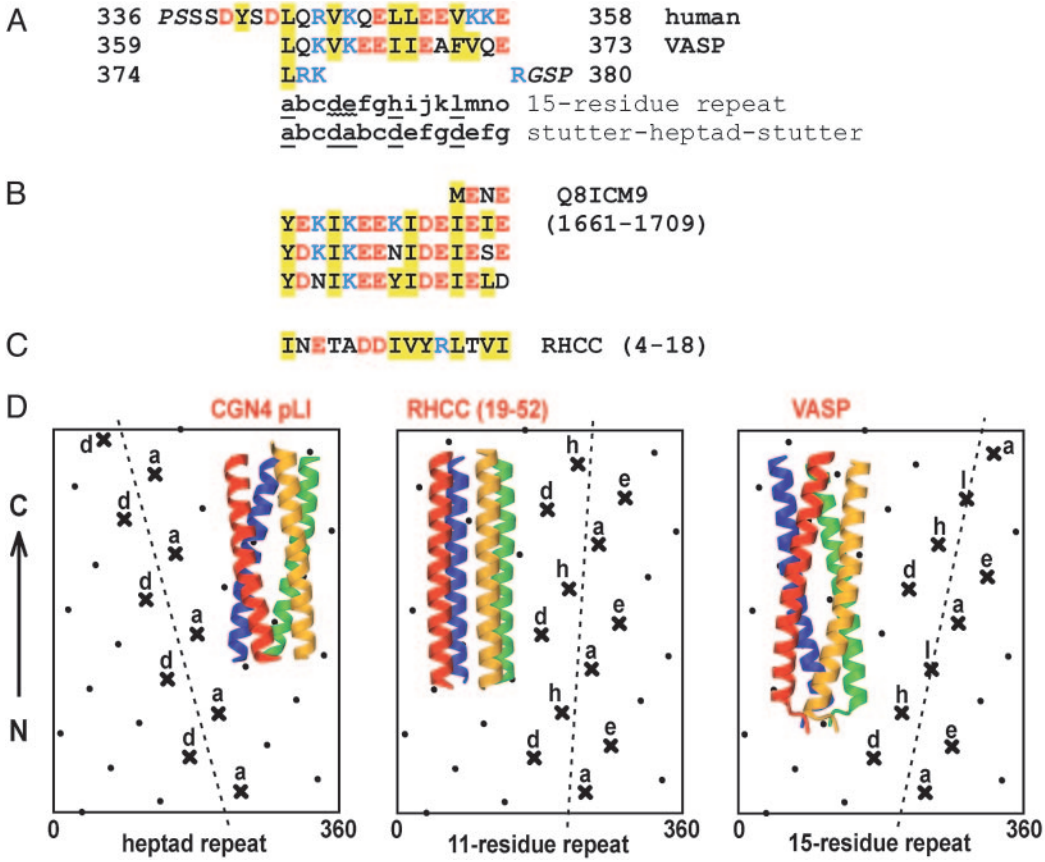

Fig. 2. The 15-residue repeat pattern. (*A*) Amino acid sequence of VASP TD formatted to highlight the 15-residue repeat pattern. Hydrophobic residues most frequently found in the hydrophobic core of coiled coils (L, V, I, and M), as well as the Y and F residues, are highlighted in yellow. Acidic residues are shown in red, and basic residues are shown in blue. Residues that are not visible in the electron density are shown in italics. The assignment of the 15-residue repeat positions is shown beneath the amino acid sequence followed by the corresponding heptad positions as assigned by TWISTER (19). Residues participating in the axial hydrophobic core are underlined. Residues in the *d* and *e* positions that form hydrophobic contacts between adjacent α-helices are underlined with a curvy line. (*B*) The sequence of residues 1,661–1,709 of the putative myosin-like protein (TrEMBL accession no. Q8ICM9) with apparent 15-residue repeats. (*C*) The sequence of residues 4–18 of the tetrabrachion fragment (8), forming a right-handed coiled-coil structure. (*D*) Helical net diagrams for the heptad, 11-residue, and 15-residue repeats. To make such a diagram, an imaginary piece of paper is wrapped around an α-helix. An arrow on the left side shows the direction of the helix from the N terminus to the C terminus. Positions forming the hydrophobic patch on the surface of the helix are marked by crosses with a dotted line showing the ''middle line'' of this patch. Color inserts show the ribbon diagrams of the GCN4-pLI leucine zipper (20) (PDB ID code 1GCL) with heptad repeats, the tetrabrachion protein (residues 19–52) (8) (PDB ID code 1FE6) with 11-residue repeats, and VASP TD.

residues show relatively large absolute values of α_{Crick} angles (Table 2) and, like the *l* layers, are instances of the knobs-to-knobs packing. Within the tetrabrachion structure, similarly organized *d*/*e* layers were observed (8). Both the *l* layers and the *d*/*e* layers are the consequences of the coiled-coil unwinding relative to the standard left-handed geometry, similar to the situation when heptad repeat stutters are present (24).

Three large cavities are found within the hydrophobic core of VASP TD on its symmetry axis. These cavities locate between layers *a* and *h* of the first repeat, between layer *h* of the first repeat and layer *a* of the second repeat and between layers *a* and *l* of the second repeat (Fig. 1*A*), and they have volumes of 370, 130, and 420 Å^3, respectively. In the four-stranded leucine zippers, cavities ranging from 30–110 Å^3 in volume were found (25), whereas the four cavities observed in the tetrabrachion fragment had volumes of 145–300 Å^3 (8). In the latter structure, clusters of five to nine water molecules were found in the cavities, but no ordered water molecules could be located within the core of VASP TD despite the high resolution. Hence, the right-handed coiled coils with either 11- or 15-residue repeats share many common features, including the organization of the hydrophobic layers as well as the presence of large cavities at the axis.

Table 2. Hydrophobic core packing of VASP TD

Position	Type of contact	Residue	α_{Crick}, °
a	Axial core	Leu-344	13.8
		Leu-359	14.1
		Leu-374	20.6
d/*e*	Next neighbor	Val-347/Lys-348	−63.8/34.7
		Val-362/Lys-363	−59.4/40.8
h	Axial core	Leu-351	−39.4
		Ile-366	−32.8
l	Axial core	Val-355	−15.0
		Phe-370	−9.6

Ionic Interactions. Charged residues account for 42% of VASP TD sequence (Fig. 2*A*). Three intrahelical and four interhelical salt bridges are observed in each of the four helices (Fig. 1*C*). In both repeats, an interhelical salt bridge between residues in the *e* and *g* positions is formed (residues Lys-348/Glu-350 and Lys-363/Glu-365, respectively). Lys-348 forms an

additional interhelical salt bridge with residue Glu-354, and residue Lys-356 simultaneously makes an intrahelical salt bridge with Glu-353 and an interhelical salt bridge with Glu-358. Last, residue Glu-373 is linked by intrahelical salt bridges to both Lys-376 and Arg-377. Like in the left-handed coiled coils (4), the extensive network of salt bridges is likely to contribute to the high stability of VASP TD.

DSC Studies. Earlier CD studies indicated that VASP TD is stable to at least 80°C in a pH range of 1–10 (9). Our DSC measurements give a midpoint melting temperature ($T_{1/2}$) of 122°C for a 0.5 mg/ml solution of VASP TD in 100 mM NaCl/20 mM Mes (pH 6.2) (Fig. 4, Table 3, and *Supporting Text*, which are published as supporting information on the PNAS web site). Repeated scans up to 130°C indicated that the unfolding process was fully reversible, whereas the transition enthalpies for consecutive scans were virtually identical. An unfolding enthalpy of 1,073 kJ/mol and a $T_{1/2}$ of 101°C for a 1 mg/ml solution was reported for a mutant ROP protein, which forms a left-handed parallel coiled-coil tetramer (26). Considering the larger length (57 residues per chain) of the ROP protein, VASP TD (45 residues) shows a comparable stability.

Residues Phe-370 found in the *l* position of the second repeat pack against each other with the smallest distance of 2.6 Å between carbon atoms (Fig. 1*B*). This phenylalanine is preserved in canine VASP, whereas it is replaced by an isoleucine in other Ena/VASP proteins. Packing of aromatic side chains into the core of four-stranded coiled coils is feasible but rare (1), whereas isoleucines and methionines are preferred in the equivalent *d* positions of the four-stranded coiled coils with heptad repeats. In VASP TD, the aromatic rings of Phe-370 are in a favorable edge-to-face π–π orientation (27, 28) (Fig. 1*B*). To evaluate the contribution of Phe-370 to the stability of VASP TD, additional DSC experiments were done with three-point mutants carrying replacements of Phe-370 by leucine, isoleucine, and alanine. Measurements in 1 M guanidine hydrochloride yielded similar unfolding enthalpies for the wild type (610 kJ/mol), Leu (618 kJ/mol), and Ile (608 kJ/mol) mutants (Fig. 4 and Table 3). In contrast, the cavity-creating mutant Phe370Ala is considerably less stable (402 kJ/mol).

Apparently, the stabilization of VASP TD by hydrophobic packing, a large contact area between the four chains and an extensive network of salt bridges is strong enough that even the presence of relatively large cavities within the hydrophobic core (which should have an adverse effect on stability) can be tolerated.

Right-Handed Coiled Coils with 15-Residue Repeats in Other Proteins. To our knowledge, VASP TD is the first right-handed coiled coil with multiple 15-residue repeats that has been analyzed in atomic detail. It may be anticipated that such coiled coils could serve as oligomerization domains in other protein families beyond the Ena/VASP family, in which the TD is highly conserved (9). Indeed, sequences with 15-residue repeats were found in other proteins (6). In particular, the YadA protein from *Yersinia pestis* (TrEMBL accession no. P31489) contains seven such repeats and was suggested to form a right-handed coiled coil (29); a small portion (10 residues) of this coiled coil was recently resolved crystallographically (30). However, the 15-residue repeats in various proteins appear to have rather heterogeneous sequences. We could find only a limited number of proteins with sequence similarity to the 15-residue repeats of human VASP in public databases, such as two unrelated putative proteins from *Plasmodium falciparum* (TrEMBL accession nos. Q8ICM9 and Q8IIG7). The Q81CM9 protein is a myosin-like protein containing three consecutive 15-residue repeats (Fig. 2*B*). Moreover, the pronounced right-handed coiled coil formed by the N-terminal region (residues 4–18) of tetrabrachion (8) has

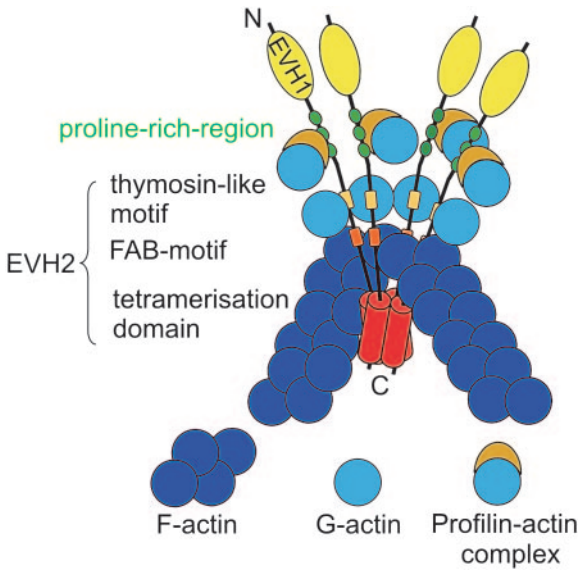

Fig. 3. Schematic representation of the full-length VASP tetramer with bound ligands.

no detectable sequence similarity to the VASP TD repeats (Fig. 2*C*), which is true also for the 15-residue repeats of the YadA protein (31). It is well established that the same three-dimensional fold is often formed by polypeptides with no apparent homology at the sequence level (32, 33). We believe that this finding may also be the case for the right-handed coiled coils with 15-residue repeats.

Biological Implications. VASP belongs to the Ena/VASP protein family that forms a key link between signaling pathways and cytoskeletal dynamics by regulating spatially confined actin-filament assembly. All members of this family consist of an N-terminal Ena-VASP homology 1 (EVH1) domain, which is a central unstructured proline-rich region of variable length, and the C-terminal EVH2 domain (34–36). The EVH2 domain contains the following three highly conserved blocks: the thymosin-like motif, which binds G-actin binding (37); the F-actin binding (FAB) motif (38–40); and the C-terminal TD, which is investigated here. The TD is required and sufficient for the tetramerization of the full-length protein (9, 38). VASP is believed to act as a molecular adaptor, and it has binding sites for various proteins. $PhePro_4$ motif containing proteins such as Zyxin, ActA, and Vinculin bind to the EVH1 domain (41), whereas profilin–actin complexes bind to several $GlyPro_5$ motifs in the proline-rich region (42).

Ena/VASP proteins are suggested to regulate actin filament by several possible mechanisms, which may depend on the model system used and include anticapping, antibranching, and profilin–actin recruitment properties (34, 36). Although some studies report that VASP antagonizes binding of capping proteins to the barbed ends of growing actin filaments and, thereby, promotes actin filament elongation (34, 43), other studies have observed inhibition of filament branching by VASP (44, 45).

As a consequence of the parallel arrangement of the C-terminal ends, the full-length tetrameric VASP adopts a "bouquet-like" structure (Fig. 3). The parallel arrangement implies an identical sequential orientation of the binding sites for EVH1 ligands, profilin–actin–ATP complexes, as well as G-actin and F-actin filaments in the intact VASP molecule. Thus, it provides high concentrations of profilin–actin–ATP complexes and G-actin in the vicinity of the uncapped barbed

ends of the growing filament. Tetravalency of ligand binding sites is expected to stabilize interactions with VASP-binding proteins. Although the biological relevance of the right-handed geometry of VASP TD is unclear, its parallel orientation would allow simultaneous binding of four actin filaments and facilitate unidirectional F-actin bundle formation. Promotion of parallel bundle formation should contribute to the high filament dynamics at the leading edge of migrating cells as well as to the initiation of filopodia formation, which are two processes in which VASP plays a key role (43, 46).

The *in vivo* importance of VASP oligomerization is emphasized by observations that C-terminal VASP fragments containing the TD perturbed various VASP-mediated F-actin assembly processes (38, 47–49), possibly due to a competition between the full-length VASP/TD heterooligomers and the full-length VASP homotetramer formation. VASP function is regulated by phosphorylation of sites in the vicinity of the actin-binding motifs (34) in response to various stimuli and cyclic nucleotide-dependent protein-kinase activation. The VASP TD structure presented here is a step toward visualization of an arrangement of VASP domains, and it suggests a model for the promotion of unidirectional actin-filament-bundle formation by VASP.

We thank Prof. Dr. T. Schwede and Dr. L. Bordoli for help with protein sequence similarity searches. We also thank Drs. R. Fedorov and W. Blankenfeldt for advice during structure refinement, Dr. R. Schröder for discussions on F-actin, and B. Voss for technical assistance. The synchrotron data collection was made possible by the European Synchrotron Radiation Facility (Grenoble, France). This work was supported in part by Deutsche Forschungsgemeinschaft SFB 355 (to T.J. and U.W.).

1. Walshaw, J. & Woolfson, D. N. (2001) *J. Mol. Biol.* **307,** 1427–1450.
2. Chothia, C., Levitt, M. & Richardson, D. (1981) *J. Mol. Biol.* **145,** 215–250.
3. Crick, F. (1953) *Acta Crystallogr.* **6,** 689–697.
4. Burkhard, P., Stetefeld, J. & Strelkov, S. V. (2001) *Trends Cell Biol.* **11,** 82–88.
5. Pauling, L., Corey, R. B. & Branson, H. R. (1951) *Proc. Natl. Acad. Sci. USA* **37,** 205–211.
6. Gruber, M. & Lupas, A. N. (2003) *Trends Biochem. Sci.* **28,** 679–685.
7. Peters, J., Baumeister, W. & Lupas, A. (1996) *J. Mol. Biol.* **257,** 1031–1041.
8. Stetefeld, J., Jenny, M., Schulthess, T., Landwehr, R., Engel, J. & Kammerer, R. A. (2000) *Nat. Struct. Biol.* **7,** 772–776.
9. Zimmermann, J., Labudde, D., Jarchau, T., Walter, U., Oschkinat, H. & Ball, L. J. (2002) *Biochemistry* **41,** 11143–11151.
10. Van Duyne, G. D., Standaert, R. F., Karplus, P. A., Schreiber, S. L. & Clardy, J. (1993) *J. Mol. Biol.* **229,** 105–124.
11. Otwinowski, Z. & Minor, W. (1997) *Macromol. Crystallogr. A* **276,** 307–326.
12. Brunger, A. T., Adams, P. D., Clore, G. M., Delano, W. L., Gros, P., Grosse-Kunstleve, R. W., Jiang, J. S., Kuszewski, J., Nilges, M., Pannu, N. S., *et al.* (1998) *Acta Crystallogr. D* **54,** 905–921.
13. Terwilliger, T. C. (2000) *Acta Crystallogr. D* **56,** 965–972.
14. Terwilliger, T. C. (2003) *Acta Crystallogr. D* **59,** 38–44.
15. Jones, T. A., Zou, J. Y., Cowan, S. W. & Kjeldgaard. (1991) *Acta Crystallogr. A* **47,** 110–119.
16. Murshudov, G. N., Vagin, A. A., Lebedev, A., Wilson, K. S. & Dodson, E. J. (1999) *Acta Crystallogr. D* **55,** 247–255.
17. Kraulis, P. J. (1991) *J. Appl. Crystallogr.* **24,** 946–950.
18. Esnouf, R. M. (1999) *Acta Crystallogr. D* **55,** 938–940.
19. Strelkov, S. V. & Burkhard, P. (2002) *J. Struct. Biol.* **137,** 54–64.
20. Harbury, P. B., Zhang, T., Kim, P. S. & Alber, T. (1993) *Science* **262,** 1401–1407.
21. Harbury, P. B., Plecs, J. J., Tidor, B., Alber, T. & Kim, P. S. (1998) *Science* **282,** 1462–1467.
22. Brown, J. H., Cohen, C. & Parry, D. A. (1996) *Proteins* **26,** 134–145.
23. Lupas, A. (1996) *Trends Biochem. Sci.* **21,** 375–382.
24. Lupas, A., Muller, S., Goldie, K., Engel, A. M., Engel, A. & Baumeister, W. (1995) *J. Mol. Biol.* **248,** 180–189.
25. Mittl, P. R., Deillon, C., Sargent, D., Liu, N., Klauser, S., Thomas, R. M., Gutte, B. & Grutter, M. G. (2000) *Proc. Natl. Acad. Sci. USA* **97,** 2562–2566.
26. Lassalle, M. W., Hinz, H. J., Wenzel, H., Vlassi, M., Kokkinidis, M. & Cesareni, G. (1998) *J. Mol. Biol.* **279,** 987–1000.
27. Hunter, C. A. & Sanders, J. K. M. (1990) *J. Am. Chem. Soc.* **112,** 5525–5534.
28. Hunter, C. A., Singh, J. & Thornton, J. M. (1991) *J. Mol. Biol.* **218,** 837–846.
29. Hoiczyk, E., Roggenkamp, A., Reichenbecher, M., Lupas, A. & Heesemann, J. (2000) *EMBO J.* **19,** 5989–5999.
30. Nummelin, H., Merckel, M. C., Leo, J. C., Lankinen, H., Skurnik, M. & Goldman, A. (2004) *EMBO J.* **23,** 701–711.
31. Lupas, A., Vandyke, M. & Stock, J. (1991) *Science* **252,** 1162–1164.
32. Murzin, A. G., Brenner, S. E., Hubbard, T. & Chothia, C. (1995) *J. Mol. Biol.* **247,** 536–540.
33. Chothia, C. (1992) *Nature* **357,** 543–544.
34. Krause, M., Dent, E. W., Bear, J. E., Loureiro, J. J. & Gertler, F. B. (2003) *Annu. Rev. Cell Dev. Biol.* **19,** 541–564.
35. Reinhard, M., Jarchau, T. & Walter, U. (2001) *Trends Biochem. Sci.* **26,** 243–249.
36. Sechi, A. S. & Wehland, J. (2004) *Front. Biosci.* **9,** 1294–1310.
37. Walders-Harbeck, B., Khaitlina, S. Y., Hinssen, H., Jockusch, B. M. & Illenberger, S. (2002) *FEBS Lett.* **529,** 275–280.
38. Bachmann, C., Fischer, L., Walter, U. & Reinhard, M. (1999) *J. Biol. Chem.* **274,** 23549–23557.
39. Huttelmaier, S., Harbeck, B., Steffens, O., Messerschmidt, T., Illenberger, S. & Jockusch, B. M. (1999) *FEBS Lett.* **451,** 68–74.
40. Laurent, V., Loisel, T. P., Harbeck, B., Wehman, A., Grobe, L., Jockusch, B. M., Wehland, J., Gertler, F. B. & Carlier, M. F. (1999) *J. Cell Biol.* **144,** 1245–1258.
41. Niebuhr, K., Ebel, F., Frank, R., Reinhard, M., Domann, E., Carl, U. D., Walter, U., Gertler, F. B., Wehland, J. & Chakraborty, T. (1997) *EMBO J.* **16,** 5433–5444.
42. Reinhard, M., Giehl, K., Abel, K., Haffner, C., Jarchau, T., Hoppe, V., Jockusch, B. M. & Walter, U. (1995) *EMBO J.* **14,** 1583–1589.
43. Bear, J. E., Svitkina, T. M., Krause, M., Schafer, D. A., Loureiro, J. J., Strasser, G. A., Maly, I. V., Chaga, O. Y., Cooper, J. A., Borisy, G. G., *et al.* (2002) *Cell* **109,** 509–521.
44. Skoble, J., Auerbuch, V., Goley, E. D., Welch, M. D. & Portnoy, D. A. (2001) *J. Cell Biol.* **155,** 89–100.
45. Samarin, S., Romero, S., Kocks, C., Didry, D., Pantaloni, D. & Carlier, M. F. (2003) *J. Cell Biol.* **163,** 131–142.
46. Svitkina, T. M., Bulanova, E. A., Chaga, O. Y., Vignjevic, D. M., Kojima, S., Vasiliev, J. M. & Borisy, G. G. (2003) *J. Cell Biol.* **160,** 409–421.
47. Grosse, R., Copeland, J. W., Newsome, T. P., Way, M. & Treisman, R. (2003) *EMBO J.* **22,** 3050–3061.
48. Vasioukhin, V., Bauer, C., Yin, M. & Fuchs, E. (2000) *Cell* **100,** 209–219.
49. Zhuang, S., Nguyen, G. T., Chen, Y., Gudi, T., Eigenthaler, M., Jarchau, T., Walter, U., Boss, G. R. & Pilz, R. B. (2004) *J. Biol. Chem.* **279,** 10397–10407.